Simulation Study of the Damage Mechanisms Appearing in a Cross Ply Composite Material Loaded in Uniaxial Tension

Eleftherios Tsivolas [1], *Leonidas N.* Gergidis[1*], *Alkiviadis S.* Paipetis[1]

[1]Department of Material Science and Engineering, University of Ioannina, 45110, Ioannina, Greece

Abstract. The objective of this paper is to predict the different damage mechanisms in multiple scales that can occur in a cross ply composite material loaded in uniaxial tension. The simulated composite material consists of four epoxy-glass fibre layers [0/90]s and the material of each layer is transversely isotropic with viscous effects that occurred from micromechanical homogenization using Mori-Tanaka formulation, extended for visco-elastic materials. For the prediction of the cracking and interlaminar delamination, cohesive contacts were used and the final crack density results were compared with the corresponding experimental ones. Finally a microscale analysis was performed in a Representative Volume Element (RVE) to observe the matrix cracking behaviour in smaller scale.

1 Introduction

Several approaches have been proposed for simulating the response of the composite materials. An important role to the accuracy of the results plays the scale (micro, meso or macro) in which the composite material has been chosen to be modeled. The smaller the scale is, the more accurate the results will be, sacrificing computational time. In micro scale, the constituents of the composite material are separately modeled, each having its own material properties. All failure mechanisms such as matrix cracking, interfacial delamination, fiber pullout, fiber fracture among others could be predicted. Using the microscale approach and solving the constitutive equations using finite element (FE) discretizations, the number of finite elements in the model increases significantly, making this option prohibitive. Another micromechanical point of view would be to consider each integration point of the (macro-scaled) composite model as a Representative Volume Element (RVE) with specific geometry and material properties and to perform a mean-field homogenization (semi-analytical homogenization techniques) at each integration point reducing the solution time of the first approach converting the solution from numerical to analytical.

* Corresponding author: lgergidi@uoi.gr

The meso-scale approach is based on modelling each layer of the composite material as a homogeneous anisotropic material ignoring the microstructure, leading to a layered structure with interfacial properties given by the user. The failure mechanisms that can appear are the layer cracking and the interfacial delamination. The macro scale approach, which is the least accurate but is preferred for large structures of composite materials is based on the actual simulation of the whole composite modelled as a homogeneous with the material properties of the whole composite. It is clear that in the aforementioned case, most of the failure mechanisms are impossible to be predicted. In the present study, a 3D mesoscale approach has been chosen, modelling each layer of the composite material as a homogenized transversely isotropic material whose elastic properties have been calculated using a two-step mean field homogenization theory. In the homogenization strategy the viscous effect of the matrix material were taken into account. Cohesive interface was used to model the interfacial properties between the layers of a [0/90]s composite material. For the simulation of the transverse cracking a large number of potential cracks were inserted at the 90o layers of the composite with the strength following a normal distribution, in order to avoid uniform stress development. Imperfection insertions such as distribution of voids could have been used, but cohesive interface was preferred for computational stability reasons. Four rows of elements through the thickness of each ply were placed to model successfully the transverse cracks. Using this method, the damage evolution sequence and the stress redistribution after each damage mechanism appearance can be predicted.

2 Modelling approach

The composite specimen modelled, is of rectangular parallelepiped shape with dimensions 30mm x 5mm x 1mm and is discretized with 96000 continuum shell elements (SC8) that can calculate accurately the transverse shear stresses. There are 4 layers through the thickness (0/90/90/0) 0.25 mm each. The composite specimen is shown in Fig. 1.

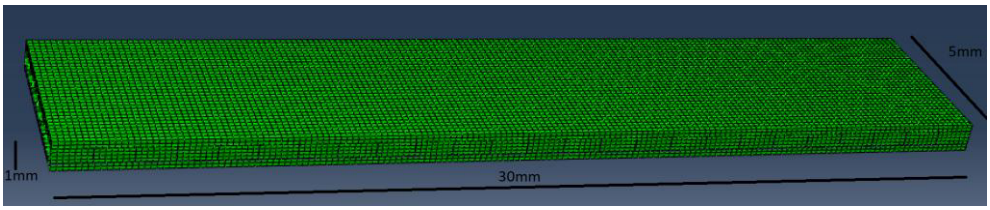

Fig. 1. Geometry and discretization of composite specimen

The material model is homogeneous linear viscoelastic that occurred from Mori Tanaka homogenisation [1], containing a linear viscoelastic matrix and elastic glass fibres. For the prediction of matrix cracking a large number of potential cracks was introduced between parts connected with cohesive contacts as shown in Fig. 2 and the strength of each contact follows a normal distribution. This method avoids the simultaneous crack opening due to the development of uniform stresses in the 90 degree layers. For the modelling of interlaminar delamination, the layers are also connected with cohesive contacts following the linear traction-separation law of equation (1):

$$\begin{Bmatrix} t_n \\ t_s \\ t_t \end{Bmatrix} = \begin{bmatrix} K_{nn} & K_{ns} & K_{nt} \\ K_{ns} & K_{ss} & K_{st} \\ K_{nt} & K_{st} & K_{tt} \end{bmatrix} \begin{Bmatrix} \delta_n \\ \delta_s \\ \delta_t \end{Bmatrix} \quad (1)$$

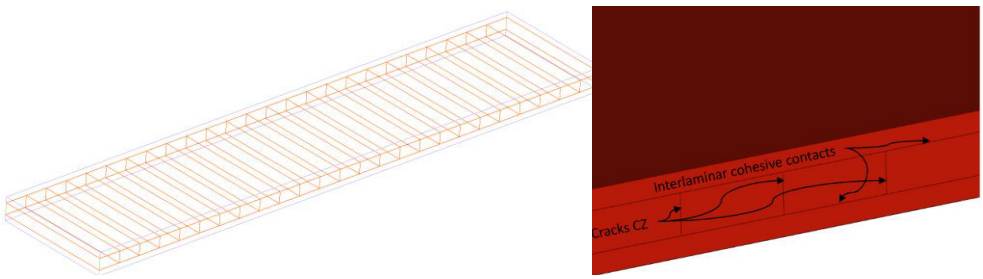

Fig. 2. Cohesive contacts for the prediction of transverse cracking and delamination. a) preview of all potential predefined cracks, b) Cohesive contacts for cracking and delamination

In the dynamic explicit analysis a total loading time of 270 seconds and total strain of 1.5% (with the displacement boundary conditions shown in Fig. 3 and numerically applied through tabular data) is adopted incrementally, with 1500 total time steps.

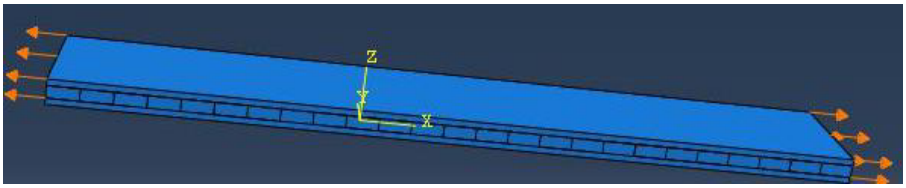

Fig. 3. Displacement boundary conditions

3 Material models

It is commonly known that the loading rate in some materials such as plastics greatly affects the mechanical response due to viscous effects. In those cases a variation of the strain rate can have great impact on the final stiffness of the material. To capture those effects various viscoelastic material models have been developed. In the present study the aforementioned effects are captured using a viscoelastic homogenization scheme taking advantage of the prony series viscoelasticity for the matrix material. The glass fibres can be considered as linear elastic in a wide range of temperatures around room temperature. The following equation describes the viscoelastic material model constitutive equation:

$$\sigma(t) = G(t) : \varepsilon(0) + \int G(t - T) : \dot{\varepsilon}^{(ve)} \tau \, d\tau \qquad (2)$$

The above linear viscoelastic equation for isotropic materials can be translated to an elastic analogous $\hat{\sigma}(s) = \hat{E}(s)\ \hat{\varepsilon}(s)$ formulation in the Laplace-Carson domain applying the transformation in the time variable for all the involved equations (constitutive equations, boundary conditions etc.), where $\hat{\sigma}$, $\hat{E}$ and $\hat{\varepsilon}$ are the transformed stress, stiffness and strain tensor in Laplace domain and s is the complex variable. The result is a fictitious RVE in this complex domain where the homogenization is performed and all the involved quantities and variables have a complex number nature. In order to get the homogenization results in the time domain an inverse Laplace-Carson transformation is required.

In Table 1 and Table 2 the material properties of each constituent are presented. In Table 3 the transversely isotropic material properties that occurred from the applied homogenization scheme are also given.

Table 1. Properties of each constituent

Property	**Matrix**	**Fibre**
Youngs Modulus (GPa)	5.5	73.1
Poisson's Ratio	0.395	0.18
Volume Fraction	-	0.63
Aspect Ratio	-	10000

Table 2. Prony series values for viscous effects of matrix material [2]

t_i(sec)	W_i
$4.949\ 10^{-8}$	$7.878\ 10^{-2}$
$7.243\ 10^{-8}$	0.2918
$9.864\ 10^{-6}$	$7.115\ 10^{-2}$
$2.8\ 10^{-3}$	0.2688
0.1644	$8.96\ 10^{-2}$
2.265	$3.018\ 10^{-2}$
35.36	$7.606\ 10^{-3}$
9368	$9.634\ 10^{-4}$
641400	$4.059\ 10^{-3}$

Table 3. Homogenized material properties occurred from Mori-Tanaka homogenization approach using the data of Table 1 and Table 2

Property	**Instantaneous**	**After 270 (seconds)**
E_1 (GPa)	48.1621	46.396
E_2 (GPa)	18.7977	3.930
ν_{12}	0.252155	0.25029
ν_{23}	0.485318	0.5658
G_{12} (GPa)	6.32782	1.255
G_{23} (GPa)	6.88076	1.415

The properties of the cohesive contacts can be seen in Table 4.

Table 4. Cohesive zone strength values taken from the literature [3]

Property	Values
Matrix Cracking (MPa)	60
Interlaminar Shear strength (MPa)	50
Fracture Energy Mode I (J/m^2) matrix cracking	500
Fracture Energy Mode II, III (J/m^2) matrix cracking	1540
Fracture Energy Mode I (J/m^2) for delamination	500
Fracture Energy Mode II, III (J/m^2) for delamination	800

4 Results

In this section the simulation results are presented. Initially, the first transverse cracks at random positions appear. As the load increases more cracks appear along with delaminations above and below the already formed cracks. Finally, after a specific number of formed cracks no other cracks can be detected due to shear lag effect [3] and crack saturation occurs. The simulation results are compared as it will be presented in the sequel with available experimental results of identical systems [5].

In Fig. 4, the CSQUADSCRT variable [4] (depicted in the colorbar) indicates whether the quadratic contact stress damage criterion has been satisfied at a contact point and it is evaluated as $(t_n/t_{n0})^2+(t_s/t_{s0})^2+(t_t/t_{t0})^2$, where t_n , t_s and t_t describe the normal and two shear tractions and t_{no}, t_{so}, and t_{to} represent the peak values of the contact stress when the separation is either purely normal to the interface or purely in the first or the second shear direction, respectively. If its value is equal to one (CSQUADSCRT=1) the criterion has been fulfilled and the contact fails.

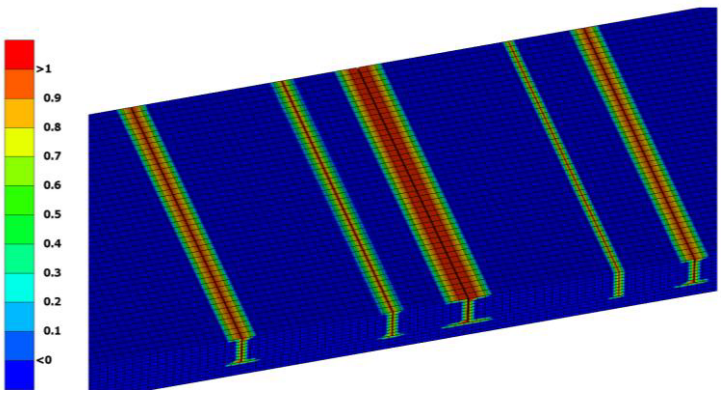

Fig. 4. Prediction of transverse cracks with cohesive zone modelling (upper layer hidden)

It is noticeable (Fig. 6) that the first cracks appearance and the saturation of the crack density occur almost for the same strain value for the simulation and the experimental data [5]. The final crack density predicted by the simulation is slightly lower than the crack density of the experiment, due to idealizations and simplification assumptions incorporated in the computational model. Also by changing the standard deviation of the distribution of the strength will result in more weak contacts for some cracks so a slightly higher final crack density can occur until saturation. The first crack occurs for a strain around 0.4% and after that point more and more cracks appear. At the second and third time steps shown in Fig. 5 the total strain is 0.5% and 0.8% respectively. For a strain around 1.2% saturation of the crack density is observed.

Fig. 5. Cracking formation and delaminations at different time steps of the analysis

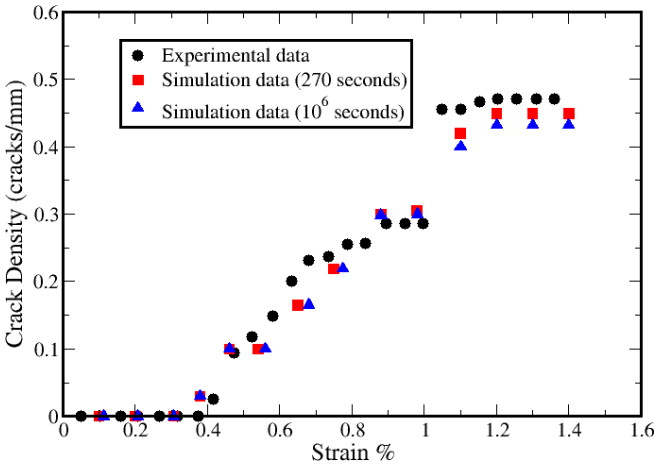

Fig. 6. Strain vs. crack density curves comparison between experimental and simulation results that consisted of a simple elastic and a viscoelastic model

5 Microscale modelling

In this chapter a micro scale analysis is presented. A RVE was generated with long glass fibres and epoxy matrix. This RVE represents an integration point of the middle layer at the crack as can be seen in Fig. 7. The boundary conditions for this RVE intimately connected with the strain tensor of the integration point chosen for the RVE. The strain tensor was

translated to displacement of the boundaries of the RVE with Dirichlet boundary conditions [6].

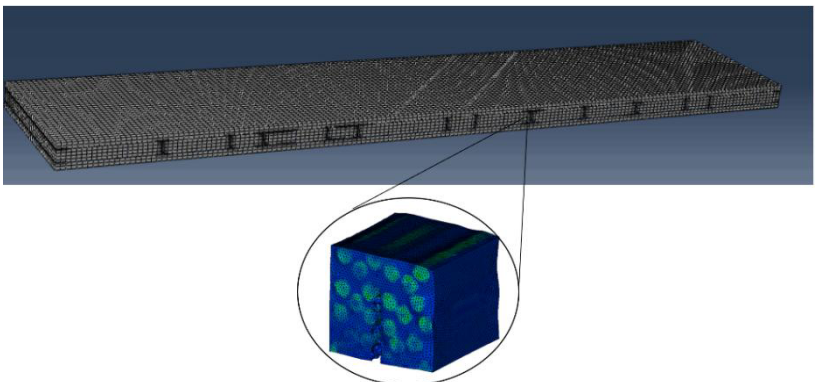

Fig. 7. RVE analysis at an integration point at the first appeared crack

In this microscale analysis the cracking simulation is based on element deletion activated by the user material (VUMAT) developed by the authors. The material of the matrix is visco-elastic with isotropic Von Mises plasticity and Chaboche isotropic damage. The fibres remain elastic. The strain tensor of the aforementioned integration point in Voigt notation is the following: $\{\varepsilon\} = [0.04956 \ \ -0.0202 \ \ -0.0214 \ \ 0.0017 \ \ 0.0002 \ \ -0.0063]$.
The cracking initiation and propagation of the matrix in different timesteps of the analysis can be seen in Fig. 8. The strain that causes the cracking initiation and the magnitude of stresses agree with the macroscale analysis.

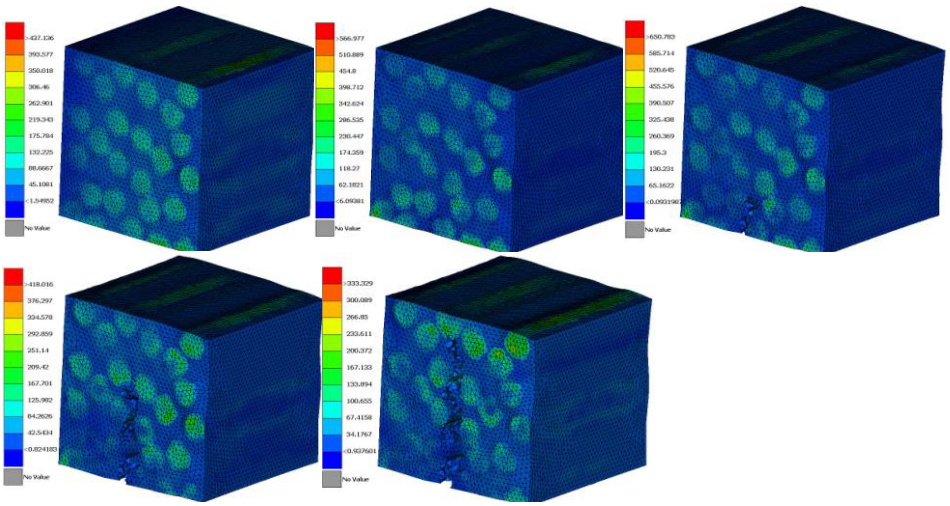

Fig. 8. RVE matrix cracking initiation and evolution

6 Conclusions

A meso and micro scale model for damage simulation of a cross ply composite is proposed. The elastic properties for each layer resulted from a homogenization procedure considering the viscous effects of the matrix for the corresponding loading time. The sample was loaded in uniaxial tension in order to identify the damage mechanisms involved. For the matrix

random cracking simulation a number or possible cracks were placed in the 90^o layers whose strength follows a normal distribution. The possible cracks and the interface are modelled using cohesive contacts. All the expected damage mechanisms appear. Stress redistributions after cracking, shear lag zone and cracking saturation are successfully simulated. Overlapping stress fields between two cracks that are very close to each other may appear too. Finally, the cracking behaviour was successfully predicted in microscale using a RVE with boundary conditions that originate from the mesoscale analysis.

References

1. C. Friebel, I. Doghri, V. Legat, Int. J. Solids Struct., **43**, 2513–2541 (2006)
2. L. Galuppi, G. Royer-Carfagni, Int. J. Solids Struct., **49**, 2637–2645 (2012)
3. Kaddour A.S, Hinton M.J, Smith P.A, and S Li. Mechanical properties and details of composite laminates for the test cases used in the third world-wide failure exercise, Journal of Composite Materials, **47**, 2427–2442 (2013)
4. J. Nairn, Mech. Mater., **26**, 63 – 80 (1997)
5. abaqus, ABAQUS/CAE user's manual, Pawtucket, RI : ABAQUS.
6. D. T. G. Katerelos, A. Paipetis, T. Loutas, G. Sotiriadis, V. Kostopoulos, S. L. Ogin, Plas. Rubber and Compos., **38**, 229–234 (2009)
7. Tsivolas, E., Gergidis, L.N., Paipetis, A.S., Key Eng. Mater., **827**, 263–268 (2019)